Original scientific paper
https://doi.org/10.33180/InfMIDEM2022.106

Informacije MIDEM
Journal of Microelectronics, Electronic Components and Materials
Vol. 52, No. 1(2022), 51 – 66

Improved Current Mode Biquadratic Shadow Universal Filter

Divya Singh, Sajal K. Paul

Department of Electronics Engineering, Indian Institute of Technology (Indian School of Mines), Dhanbad, Jharkhand, India

Abstract: In this paper, an improved single-input-multiple-output (SIMO) current-mode biquadratic shadow universal filter (SUF) is realized using two new variants of second-generation current conveyors (CCIIs), namely current conveyor cascaded transconductance amplifier (CCCTA) and extra-X current controlled conveyor transconductance amplifier (EX-CCCTA). The low pass and the band pass outputs of a non-shadow universal filter (NSUF), consisting of CCCTA, are utilized through two amplifiers' feedback paths using one EX-CCCTA to realize the proposed SUF. It is resistorless and utilizes only two grounded capacitors. All the five standard responses of SUF, such as low pass (LP), high pass (HP), band pass (BP), band-reject (BR), and all pass (AP), are obtained simultaneously. The main advantage of SUF over NSUF is the ease of orthogonal tuning of the pole frequency (ω_o) and quality factor (Q_o) with the bias currents of CCCTA and EX-CCCTA. It is suitable for full cascadability because of proper input and output impedances. Moreover, it simplifies integrated circuit implementation because all capacitors are grounded and no resistors are required. It does not possess any component matching constraints and consumes 4.1mW of power. The theoretical results have been validated in TSMC 180nm technology using Cadence Virtuoso.

Keywords: CCCTA; EX-CCCTA; CCII; CM universal filter; CM shadow universal filter

Izboljšan tokovni bikvadrantni univerzalni filter v senci

Izvleček: V tem članku je izboljšan enovhodno-večizhodni (SIMO) tokovni bikvadratni univerzalni filter v senci (SUF) z uporabo dveh novih različic tokovnih pretvornikov druge generacije (CCII), in sicer kaskadnega transkonduktančnega ojačevalnika (CCCTA) in transkonduktančnega ojačevalnika z nadzorom toka (EX-CCCTA). Izhodi nizkoprepustnega in pasovnega prehoda univerzalnega filtra brez sence (NSUF), ki ga sestavlja CCCTA, se uporabljajo prek dveh povratnih poti am-prevodnikov z uporabo enega EX-CCCTA za izvedbo predlaganega SUF. Filter je brez uporov in uporablja le dva ozemljena kondenzatorja. Vseh pet standardnih odzivov SUF, kot so nizka prepustnost (LP), visoka prepustnost (HP), pasovna prepustnost (BP), zavrnitev pasu (BR) in celotna prepustnost (AP), se dobi hkrati. Glavna prednost SUF pred NSUF je enostavnost ortogonalnega nastavljanja polne frekvence (ω_o) in faktorja kakovosti (Q_o) z diagonalnimi tokovi CCCTA in EX-CCCTA. Zaradi ustreznih vhodnih in izhodnih impedanc je primeren za popolno kaskadnost. Poleg tega poenostavlja izvedbo integriranih vezij, saj so vsi kondenzatorji ozemljeni in upori niso potrebni. Nima nobenih omejitev glede usklajevanja komponent in porabi le 4,1 mW energije. Teoretični rezultati so bili potrjeni v 180 nm tehnologiji TSMC z uporabo programa Cadence Virtuoso.

Ključne besede: CCCTA; EX-CCCTA; CCII; CM univerzalni filter; CM universal filter v senci

** Corresponding Author's e-mail: sajalkpaul@rediffmail.com*

1 Introduction

Current-mode (CM) universal filters, especially the single-input multiple-output (SIMO) type, have received significant attention [1-3] because of their wide applications. They are useful for many applications, namely communication systems, instrumentation, control systems,

How to cite:
D. Singh et al., "Improved Current Mode Biquadratic Shadow Universal Filter", Inf. Midem-J. Microelectron. Electron. Compon. Mater., Vol. 52, No. 1(2022), pp. 51–66

signal generation, and signal processing. Moreover, the possibility of simultaneous realization of multiple filter functions with the same topology finds use in PLL FM demodulator, touch-tone phone, and crossover network used in a three-way high-fidelity loud-speaker [4]. A reasonably good filter should have the following important features: simultaneous realization of various filter responses, use of few active and passive components, full cascadability i.e., low input impedance and high output impedance, all grounded components, low space requirement, no component matching constraints, low sensitivity, low power consumption, ease of orthogonal adjustment of pole frequency (ω_o) and quality factor (Q_o) including electronic tuning of various parameters. It may be appreciated that among the many parameters, the orthogonal tuning of ω_o and Q_o and electronic tuning plays a crucial role, primarily when the filter is implemented as an integrated circuit (IC). The literature survey reveals that many biquadratic current mode filters lack orthogonal electronic tuning capability.

Shadow filters introduce simple orthogonal electronic tuning of ω_o and Q_o of a core filter via amplifier gain. Lakys and Fabre [5, 6] introduced the shadow filter (also termed as frequency-agile filter) in 2010, where the low pass output of a second order core filter (non-shadow filter) is fed back to the input through an amplifier. This resulted in capability to control ω_o and Q_o (but not bandwidth (BW)) via gain; moreover, ω_o and Q_o cannot be tuned independently. Biolkova and Biolek [7] extended the idea, as shown in Fig. 1, and achieved an enhanced flexibility in the control of ω_o, Q_o and BW of the filter by gain of one or more feedback amplifier(s) connected externally [7].

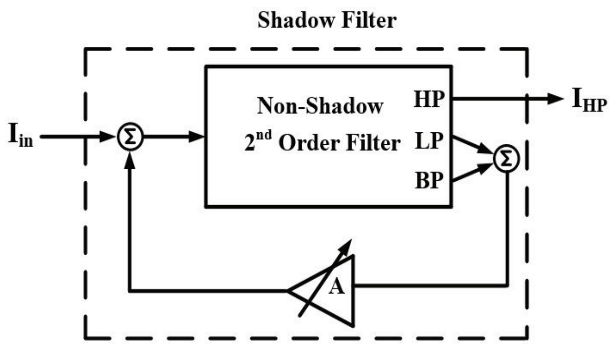

Figure 1: Scheme of Shadow filter [6].

A large diversity of SIMO filters are reported [1-4, 8-43]. Filter topologies [1-4, 8-28] are non-shadow (NS) type, while filter topologies [29-43] are shadow (S) type. Further, [29-35] are current-mode (CM) types and [36-43] are voltage-mode (VM) types.

In [1], non-shadow universal filters (NSUF) using four CFTAs and two grounded capacitors are reported. However, the simultaneous UF responses and ease of orthogonal tuning of ω_o and Q_o are not possible [1]. The topology [2] uses two CCCIIs, one MO-CCCA, and two grounded capacitors. In [3], four MO-OTAs are used. It has the following shortcomings: it does not possess full cascadability, requires matching constraints for UF realization, and independent control of ω_o and Q_o is not possible for the LP filter. In [4], an NSUF using three differential voltage current conveyors (DVCCs) and six passive elements without full cascadability is presented. In [8], the LP, HP, and BP filter are realized using one current follower transconductance amplifier (CFTA). However, one output is obtained through a capacitor; hence its practical implementation needs additional circuitry. A single current conveyor transconductance amplifier (CCTA) based NSUF is implemented in [9]. Again, a universal filter is reported with three DVCCs and six MOS resistors [10] without simultaneous responses and electronic tunability. Two operational transconductance amplifiers (OTAs) based NSUF circuit is presented in [11]. Moreover, NSUF in [12], using four Z-copy current follower transconductance amplifiers (ZC-CFTAs), provides simultaneous responses. On the other hand, NSUF using two Z-copy current inverter transconductance amplifiers (ZC-CITAs) is implemented in [13]. In [14], three MOCCCIIs are used, but the circuit does not provide full cascadability and ease of orthogonality. Further, one voltage differencing gain amplifier (VDGA) along with two resistors and capacitors are used for implementing multifunctional filters [15]. In [16], a universal filter without independent tunability is reported by employing two extra X current conveyor transconductance amplifier and six passive elements. Three/four second-generation current-controlled conveyors (DOCCCIIs/CCCIIs) [17, 19, 21] and three ZC-CFTAs [20] with minimal passive elements are used to realize NSUFs with simultaneous responses. In [18], a universal filter is reported consisting of one dual-X current conveyor transconductance amplifier (DXCCTA) with three passive elements. Furthermore, an NSUF is reported in [22] using two OTAs and one third-generation current conveyor (CCIII) with three passive elements. A universal filter [23] with two DVCCs and five passive components is reported. In [24], a multifunction filter is realized using voltage differencing dual X current conveyor with two grounded capacitors and two grounded resistors. Moreover, two multiple-output-operational floating conveyors (MOOFCs) with four passive elements provide an NSUF [25] with no simultaneous responses. A BJT-based universal filter is realized in [26] with two grounded capacitors. Moreover, an NSUF using a single VDTA and three passive components is reported in [27]. A universal filter is realized in [28] without full cascadability and ease of independent tunability. The available shadow filters (SFs) are reported [29-43]. The CDTA/VDTA based shadow filters [29] realize only LP and BP through the capacitor with no full casacadability. Further, the shadow filter topology [30] reports only BP response utilizing a capacitor, but without full cascadability and orthogonal tuning of ω_o and Q_o. Moreover, shadow filter topology [31] realizes multifunction filters (LP, BP, and HP) using three CDTAs. However, the obtained BP and HP current signal conducted through a series capacitor to ground and hence extra circuitry is required to use these responses practically. It does not have the ease of cascadability and orthogonal tunability. Four OFCCs with five resistors and two capacitors implement a shadow BP filter [32] with no electronic tuning. Similarly, a BP filter with two CDTAs, one current amplifier (CA), and two capacitors is implemented [33]. Another shadow BP filter using four ECCII and four passive elements is reported [34] without full cascadability and electronic tuning. In [35], two CM shadow filters are reported. The first is a multifunction filter (LP, HP, and BP) using two CC-CDCTAs and two grounded capacitors. However, the obtained HP current signal conducted through a series capacitor to ground, and hence extra circuitry is required as of to use it practically. The second one is a shadow UF (SUF) using three CC-CDCTA, one CCCII, and two capacitors, of which one is floating. This is probably the first reported CM SUF. In [36, 43], VM shadow filters are comprised with differential difference current conveyor with higher number of passive elements without full cascadability. Op-amps are employed [37] to realize multifunction VM shadow filter with limitations on gain-bandwidth product and slew rate. Current feedback operational amplifiers (CFOAs) with higher number of passive elements are utilized to realize a multifunctional VM filter without simultaneous responses in [38] and single response filter in [39, 40]. In [41], three operational transresistance amplifiers (OTRAs) with eleven resistors and four capacitors are employed and provide only low-pass and band-pass responses. A VM shadow filter is realized in [42] using three voltage differencing differential-difference amplifiers (VDDDAs). To our best knowledge the work [42] reports the first VM shadow universal filter.

This paper describes a realization of an improved resistorless biquadratic current mode SUF. It uses two modified active building blocks, namely current conveyor cascaded transconductance amplifier (CCCTA) and extra-X current controlled conveyor transconductance amplifier (EX-CCCTA). The proposed shadow filter possesses the following advantageous features: simultaneous realization of various filter responses without alteration of the circuit, no component matching constraints, use of only two ABBs and two grounded capacitors, it is resistorless, fully cascadable, has low sensitivity and low power consumption, provides the possibility of orthogonally adjustment of the pole frequency (ω_o) and the quality factor (Q_o) including electronic tuning of various parameters, and is suitable for integrated circuit implementation. To distinguish the similar mathematical and non-mathematical symbols with reference to both the blocks, superscripts (1) and (2) have been used all through the paper for the CCCTA and EX-CCCTA, respectively. Such as, $M_1^{(1)}$, $g_{m1}^{(1)}$ and $I_Y^{(1)}$ represent for CCCTA while $M_{20}^{(2)}$, $g_{m1}^{(2)}$ and $I_Y^{(2)}$ represent for EX-CCCTA.

This paper consists of six sections. Section 1 gives the introduction, followed by Section 2, which describes active building blocks. Section 3 discusses the proposed universal shadow filter and its analysis. Section 4 gives the non-ideality analysis while the proposed circuit is compared to existing filters in section 5. Verification through simulation and experimentation is given in section 6 and section 7, respectively, followed by the conclusion in section 8.

2 Active building blocks

In this section, two active building blocks, CCCTA and EX-CCCTA, are being discussed. These building blocks are used for UF realization.

2.1 Current conveyor cascaded transconductance amplifier (CCCTA)

The second-generation current conveyor (CCII) is a well-known current mode building block. The CCII structure has two input terminals, X and Y, at low and high impedance respectively, and one high impedance output terminal, Z. In [44], a BJT based CCII is modified into a current conveyor transconductance amplifier (CCTA) by the addition of transconductance amplifier (TA) at the Z terminal of CCII in series. This paper proposes a new variant of CCII, composed of CCTA followed by an additional TA in cascade resulting in a current conveyor cascaded transconductance amplifier (CCCTA). The symbol of the proposed CCCTA is shown in Fig. 2, and its CMOS-based internal structure is shown in Fig. 3. The first stage, CCII, is composed of $M_1^{(1)}$ - $M_9^{(1)}$, and after that, two TA stages, formed by $M_{10}^{(1)}$ - $M_{17}^{(1)}$, are cascaded.

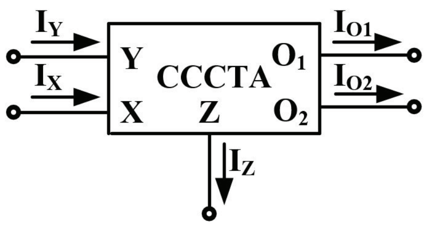

Figure 2: Symbol of CCCTA.

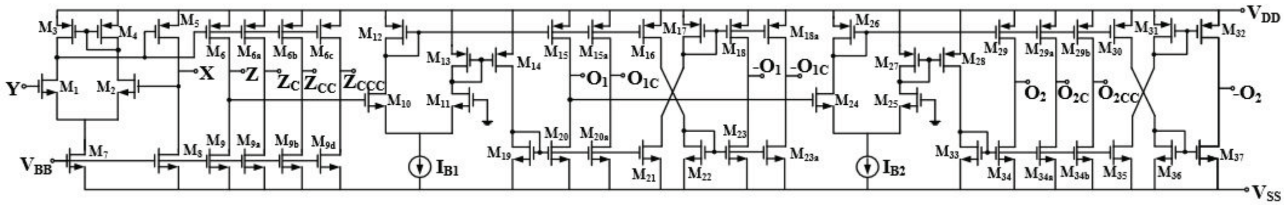

Figure 3: The CMOS-based Internal structure of CCCTA

The port relationships for CCCTA are given as follows:

$$\begin{bmatrix} I_Y^{(1)} \\ V_X^{(1)} \\ I_Z^{(1)} \\ I_{O1}^{(1)} \\ I_{O2}^{(1)} \end{bmatrix} = \begin{bmatrix} 0 & 0 & 0 & 0 & 0 \\ 1 & 0 & 0 & 0 & 0 \\ 0 & 1 & 0 & 0 & 0 \\ 0 & 0 & g_{m1}^{(1)} & 0 & 0 \\ 0 & 0 & 0 & g_{m2}^{(1)} & 0 \end{bmatrix} \begin{bmatrix} V_Y^{(1)} \\ I_X^{(1)} \\ V_Z^{(1)} \\ V_{O1}^{(1)} \\ V_{O2}^{(1)} \end{bmatrix} \quad (1)$$

Where $g_{m1}^{(1)}$ d $g_{m2}^{(1)}$ are the transconductances of the first and second TA, respectively. They can be expressed as:

$$g_{m1}^{(1)} = \sqrt{\mu_n C_{ox} \left(\frac{W}{L}\right)_{M_{10}^{(1)},\ M_{11}^{(1)}} I_{B1}} \quad (2a)$$

$$g_{m2}^{(1)} = \sqrt{\mu_n C_{ox} \left(\frac{W}{L}\right)_{M_{14}^{(1)},\ M_{15}^{(1)}} I_{B2}} \quad (2b)$$

Where μ, C_{ox}, W/L, I_{B1}, and I_{B2} have their usual meaning. The proposed CCCTA is designed in TSMC 180 nm technology. The aspect ratios of transistors are given in Table 1.

Table 1: The aspect ratio of MOS Transistors of CCCTA.

MOS Transistors	W(μm)/ L(μm)	MOS Transistors	W(μm)/ L(μm)
$M_{1,7}^{(1)}$	7.2/0.36	$M_{5,6}^{(1)}$	6.12/0.36
$M_{2}^{(1)}$	19.6/0.36	$M_{8,9}^{(1)}$	31.6/0.36
$M_{3,4}^{(1)}$	3.6/0.36	$M_{10-37}^{(1)}$	10.8/0.36

The essential features of the CCCTA in Fig. 2 can be verified through simulation. The dc current and voltage characteristics, $I_Z^{(1)}$ versus $I_X^{(1)}$ and $V_X^{(1)}$ versus $V_Y^{(1)}$, are shown in Fig. 4. The dc current characteristic is almost linear for the range of -376 μA to 500 μA while the dc voltage characteristic is linear for the range of -1.14 V to 1.14 V. Fig. 5 shows the frequency response of current gains, $I_Z^{(1)}/I_X^{(1)}$, $I_{O1}^{(1)}/I_X^{(1)}$, and $I_{O2}^{(1)}/I_X^{(1)}$ with a -3 dB bandwidths being 1.4 GHz, 45.7 MHz, and 45.7 MHz, respectively. It is observed from Fig. 5 (b) that the gains $I_{O1}^{(1)}/I_X^{(1)}$ and $I_{O2}^{(1)}/I_X^{(1)}$ overlap. Table 2 summarizes the performance parameters of CCCTA.

(a)

(b)

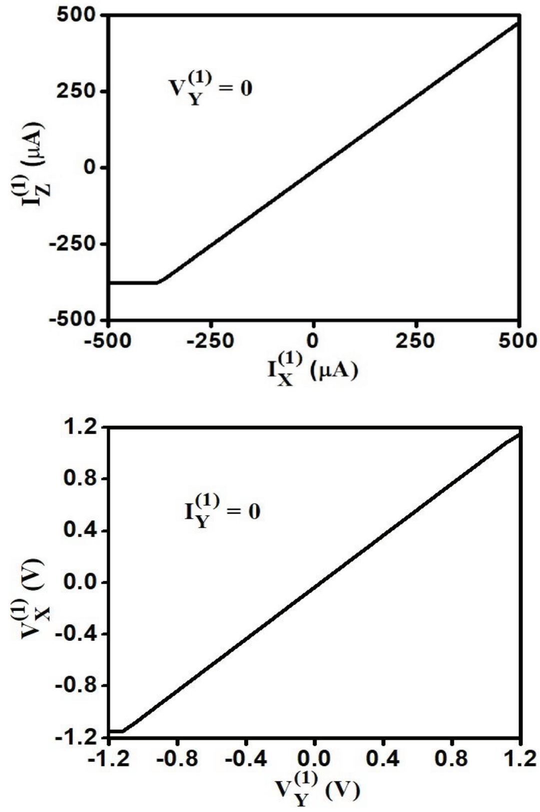

Figure 4: The plot of dc characteristics (a) I_Z versus I_X (b) V_X versus V_Y.

2.2 Extra-X second generation current controlled conveyor transconductance amplifier (EX-CCCTA)

Extra X- second generation current controlled conveyor (EX-CCCII) is one of the variants of CCCII, which adds one more X terminal and, therefore, extra intrinsic resistance at X terminal. This paper introduces a new variant of CCCII, an extra-X second-generation current controlled conveyor transconductance amplifier (EX-CCCTA), in which two TAs are connected at two Z terminals. The symbol of EX-CCCTA is shown in Fig. 6, and its CMOS internal structure, as shown in Fig. 7, is modified from ref. [45].

(a)

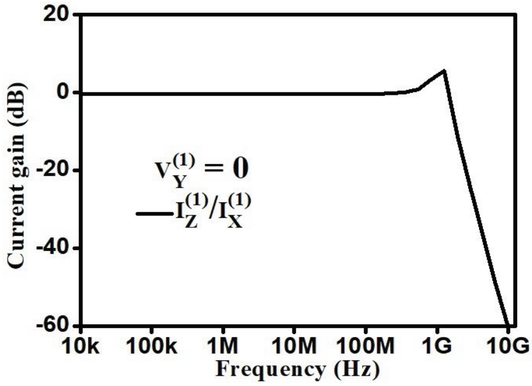

(b)

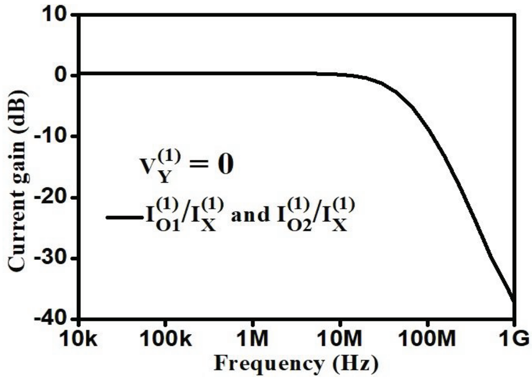

Figure 5: Current gain frequency response at (a) Z, (b) O_1 and O_2

Table 2: Performance parameters of CCCTA.

Parameters	Values
Supply Voltage	± 1.5 V
Power Consumption for V_{BB} = -1 V, $I_{B1} = I_{B2}$ = 56 µA	3.6 mW
Parasitics at Y port ($R_Y^{(1)}$, $C_Y^{(1)}$)	360 kΩ, 2.73 fF
Parasitics at X port ($R_X^{(1)}$)	679 Ω
Parasitics at Z port ($R_Z^{(1)}$, $C_Z^{(1)}$)	4.38 MΩ, 4.12 fF
Parasitics at O_1 port ($R_{O1}^{(1)}$, $C_{O1}^{(1)}$)	2.54 MΩ, 3.42 fF
Parasitics at O_2 port ($R_{O2}^{(1)}$, $C_{O2}^{(1)}$)	2.3 MΩ, 3.24 fF
Linear variation of $I_Z^{(1)}$ over $I_X^{(1)}$	-376 µA to 500 µA
Linear variation of $V_X^{(1)}$ over $V_Y^{(1)}$	-1.14 V to 1.14 V
Bandwidth of $I_Z^{(1)} / I_X^{(1)}$	1.4 GHz
Bandwidth of $I_{O1}^{(1)} / I_X^{(1)}$	45.7 MHz
Bandwidth of $I_{O2}^{(1)} / I_X^{(1)}$	45.7 MHz

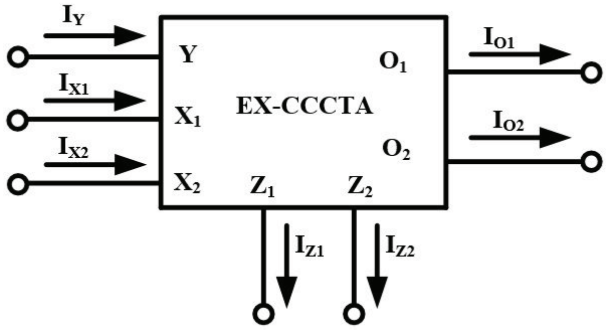

Figure 6: Symbol of EX-CCCTA.

The port relationships for EX-CCCTA are as follows:

$$\begin{bmatrix} I_Y^{(2)} \\ V_{X1}^{(2)} \\ V_{X2}^{(2)} \\ I_{Z1}^{(2)} \\ I_{Z2}^{(2)} \\ I_{O1}^{(2)} \\ I_{O2}^{(2)} \end{bmatrix} = \begin{bmatrix} 0 & 0 & 0 & 0 & 0 & 0 & 0 \\ 1 & R_{X1}^{(2)} & 0 & 0 & 0 & 0 & 0 \\ 1 & 0 & R_{X2}^{(2)} & 0 & 0 & 0 & 0 \\ 0 & 1 & 0 & 0 & 0 & 0 & 0 \\ 0 & 0 & 1 & 0 & 0 & 0 & 0 \\ 0 & 0 & 0 & g_{m1}^{(2)} & 0 & 0 & 0 \\ 0 & 0 & 0 & 0 & g_{m2}^{(2)} & 0 & 0 \end{bmatrix} \begin{bmatrix} V_Y^{(2)} \\ I_{X1}^{(2)} \\ I_{X2}^{(2)} \\ V_{Z1}^{(2)} \\ V_{Z2}^{(2)} \\ V_{O1}^{(2)} \\ V_{O2}^{(2)} \end{bmatrix} \quad (3)$$

$R_{X1}^{(2)}$ and $R_{X2}^{(2)}$ are the intrinsic resistances at the X_1 and X_2 terminals, respectively. Parasitics at Y port are given by ($R_Y^{(2)}$, $C_Y^{(2)}$). Similarly, $g_{m1}^{(2)}$ and $g_{m2}^{(2)}$ are the transconductances of the first and second TA. Values of $R_{X1}^{(2)}$ and $R_{X2}^{(2)}$ can be computed as:

$$R_{X1}^{(2)} = R_{X2}^{(2)} \cong \frac{1}{\sqrt{2I_{C1}C_{OX}}\left(\sqrt{\frac{\mu_p W_p}{L_p}} + \sqrt{\frac{\mu_n W_n}{L_n}}\right)} \quad (4)$$

The values of $R_{X1}^{(2)}$ and $R_{X2}^{(2)}$ are equal when $\left(\frac{W}{L}\right)_{M_2^{(2)}} = \left(\frac{W}{L}\right)_{M_3^{(2)}}$ and $\left(\frac{W}{L}\right)_{M_5^{(2)}} = \left(\frac{W}{L}\right)_{M_6^{(2)}}$.

The analysis of the operational transconductance amplifier yields

$$g_{m1}^{(2)} = \sqrt{\mu_n C_{ox}\left(\frac{W}{L}\right)_{M_{20}^{(2)},\ M_{21}^{(2)}} I_{C2}} \quad (5a)$$

$$g_{m2}^{(2)} = \sqrt{\mu_n C_{ox}\left(\frac{W}{L}\right)_{M_{24}^{(2)},\ M_{25}^{(2)}} I_{C3}} \quad (5b)$$

Where μ is the mobility, C_{OX} is the oxide capacitance, W/L is the aspect ratio and I_{C2}, I_{C3} are the bias currents. The proposed EX-CCCTA is designed in TSMC 180 nm CMOS technology, the aspect ratios of transistors are given in Table 3.

Table 3: The aspect ratio of EX-CCCTA of Fig. 7.

MOS Transistors	W(μm)/ L(μm)	MOS Transistors	W(μm)/ L(μm)
$M^{(2)}_{1,\,2,\,3}$	11.5/0.36	$M^{(2)}_{13-19}$	4.5/0.36
$M^{(2)}_{4-12}$	7.2/0.36	$M^{(2)}_{20-43}$	10.8/0.36

The basic architecture of EX-CCCTA is similar to CCCTA. Hence, the simulated responses of EX-CCCTA are the same as the responses of the CCCTA block.

3 Proposed shadow filter realization

The shadow filter implementation using two feedback amplifiers, as given in Fig. 1 [6], is adopted in this paper to improve the non-shadow filter performance. The band pass and low pass responses of the non-shadow filter are fed back to the input through amplifiers A_1 and A_2, respectively. The shadow universal filter (SUF) realization, in line with Fig. 1, is shown in Fig. 8. One of the constituents of it is NSUF, shown inside the small dotted lines. Hence, at first, we briefly discuss NSUF realization, followed by the realization of SUF.

The proposed SIMO current mode (CM) second-order NSUF using a single CCCTA and two grounded capacitors is shown in Fig. 8 inside the small dotted lines. Where $Z^{(1)}_{C}$, $Z^{(1)}_{CC}$, and $Z^{(1)}_{CCC}$ are the $Z^{(1)}$ copies. The $O^{(1)}_{1C}$, and $O^{(1)}_{1CC}$, are $O^{(1)}_{1}$ copies, and similarly, $O^{(1)}_{2}$ copies are represented. The current at terminals $-O^{(2)}_{1}$ and $-O^{(2)}_{2}$ is 180 degree phase shifted over $O^{(2)}_{1}$ and $O^{(2)}_{2}$ terminals, respectively. The proposed filter provides all the standard UF responses such as low pass, band pass, high pass, band-reject, and all pass simultaneously. It has low input impedance and high output impedances, suitable for full cascading in the current mode. The routine analysis of NSUF results in the pole frequency and quality factor as:

$$Pole\ freq. = \sqrt{\frac{g^{(1)}_{m1} g^{(1)}_{m2}}{C_1 C_2}},\ Q.\ factor = \sqrt{\frac{C_1 g^{(1)}_{m2}}{C_2 g^{(1)}_{m1}}} \qquad (6)$$
$$Bandwidth = \frac{g^{(1)}_{m1}}{C_1}$$

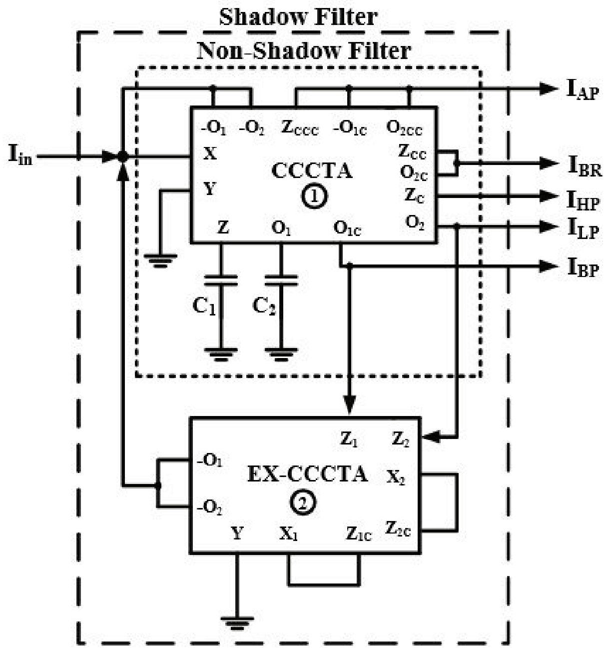

Figure 8: Proposed Shadow universal filter.

Equation (5) indicates that the pole frequency, quality factor, and bandwidth are electronically tunable by bias currents because of $g^{(1)}_{m1}$ and $g^{(1)}_{m2}$. Moreover, pole frequency can easily be tuned independently of quality factor by varying $g^{(1)}_{m1} = g^{(1)}_{m2} = g_m$ with bias currents. However, the quality factor cannot be tuned independently of pole frequency easily.

It is also observed from Fig. 8 that the proposed SUF is realized with CCCTA based NSUF and EX-CCCTA. The two current amplifiers A_1 and A_2, are implemented using one EX-CCCTA. The amplifier gains are expressed as $A_1 = g^{(2)}_{m1} R^{(2)}_{X1}$ and $A_2 = g^{(2)}_{m2} R^{(2)}_{X2}$, where $g^{(2)}_{m1}$ and $g^{(2)}_{m2}$ are

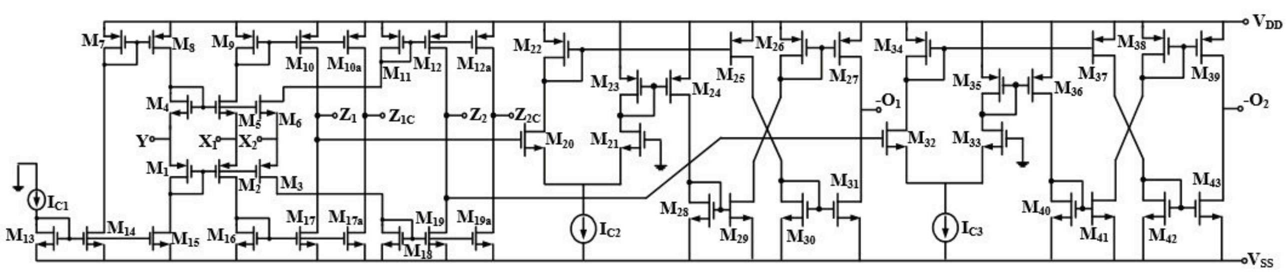

Figure 7: The CMOS-based internal structure of EX-CCCTA.

the first and second transconductances of the second analog building block (ABB), EX-CCCTA.

Thereafter, the routine analysis of the circuit of Fig. 8 results in the transfer functions as follows:

$$\frac{I_{LP}}{I_{in}} = \frac{g_{m1}^{(1)} g_{m2}^{(1)}}{D(s)} \tag{7}$$

$$\frac{I_{BP}}{I_{in}} = \frac{sC_2 g_{m1}^{(1)}}{D(s)} \tag{8}$$

$$\frac{I_{HP}}{I_{in}} = \frac{s^2 C_1 C_2}{D(s)} \tag{9}$$

$$\frac{I_{BR}}{I_{in}} = \frac{s^2 C_1 C_2 + g_{m1}^{(1)} g_{m2}^{(1)}}{D(s)} \tag{10}$$

$$\frac{I_{AP}}{I_{in}} = \frac{s^2 C_1 C_2 - sC_2 g_{m1}^{(1)} + g_{m1}^{(1)} g_{m2}^{(1)}}{D(s)} \tag{11}$$

where,

$$D(s) = s^2 C_1 C_2 + sC_2 g_{m1}^{(1)} (1 + A_1) + g_{m1}^{(1)} g_{m2}^{(1)} (1 + A_2) \tag{12}$$

The equations (7) – (11) show that all the standard responses of SUF such as low pass (LP), high pass (HP), band pass (BP), band-reject (BR), and all pass (AP) have been realized simultaneously.

The above transfer functions results in the following gains:

$$A_{LP} = A_{BR} = \frac{1}{1 + A_2}, A_{BP} = \frac{1}{1 + A_1}, A_{HP} = A_{AP} = 1 \tag{13}$$

The denominator of the above transfer functions results in the pole frequency (ω_o), quality factor (Q_o) and the bandwidth (BW) of the SUF given by:

$$\omega_o = \sqrt{\frac{g_{m1}^{(1)} g_{m2}^{(1)} (1 + A_2)}{C_1 C_2}} \tag{14a}$$

$$Q_o = \frac{1}{(1 + A_1)} \sqrt{\frac{C_1 g_{m2}^{(1)} (1 + A_2)}{C_2 g_{m1}^{(1)}}} \tag{14b}$$

$$BW = \frac{g_{m1}^{(1)} (1 + A_1)}{C_1} \tag{14c}$$

If $g_{m1}^{(1)} = g_{m2}^{(1)} = g_m$ and $C_1 = C_2 = C$, then the above equation can be rewritten as:

$$\omega_o = \frac{g_m}{C} \sqrt{(1 + A_2)}\ , Q_o = \frac{\sqrt{(1 + A_2)}}{(1 + A_1)} \tag{15a}$$

$$BW = \frac{g_m (1 + A_1)}{C} \tag{15b}$$

The sensitivity analysis of ω_o, Q_o, and BW using (14) results in:

$$S_{g_{m1}^{(1)}}^{\omega_o} = S_{g_{m2}^{(1)}}^{\omega_o} = \frac{1}{2}, \quad S_{C_1}^{\omega_o} = S_{C_2}^{\omega_o} = -\frac{1}{2}, \quad S_{g_{m2}^{(2)}}^{\omega_o} = S_{R_{X2}^{(2)}}^{\omega_o} = \frac{1}{2}\left(\frac{A_2}{1 + A_2}\right) \tag{16}$$

$$S_{g_{m1}^{(2)}}^{Q_o} = S_{R_{X1}^{(2)}}^{Q_o} = -\frac{A_1}{1 + A_1}, S_{C_1}^{Q_o} = S_{g_{m2}^{(1)}}^{Q_o} = \frac{1}{2}, \quad S_{C_2}^{Q_o} = S_{g_{m1}^{(1)}}^{Q_o} = -\frac{1}{2}, S_{g_{m2}^{(2)}}^{Q_o} = S_{R_{X2}^{(2)}}^{Q_o} = \frac{1}{2}\left(\frac{A_2}{1 + A_2}\right) \tag{17}$$

$$S_{g_{m1}^{(2)}}^{BW} = S_{R_{X1}^{(2)}}^{BW} = -\frac{A_1}{1 + A_1}, S_{g_{m1}^{(1)}}^{BW} = 1, S_{C_1}^{BW} = -1 \tag{18}$$

It is observed from equation (15) that Q_o can be adjusted independently of ω_o by electronically controlling the value of A_1 with $g_{m1}^{(2)}$. Similarly, ω_o can be adjusted independently of Q_o by electronically controlling g_m. Also, BW can be electronically controlled independently of ω_o by controlling A_1 with $g_{m1}^{(2)}$. Furthermore, BW can be tuned independently from Q_o via g_m. It is also evident from equation (13) that AP, BP, and BR gains can be electronically controlled with A_1 and A_2. The sensitivities of all the parameters are within unity in magnitude irrespective of the value of A_1 and A_2. Thus, the most important achievement of SUF over NSUF is the ease of orthogonal adjustment of pole frequency and quality factor.

4 Non-ideality analysis

Practically there will be effects of non-ideal transfer gains and parasitics of active building blocks. The effects of these two types of non-idealities are discussed in section 4.1 and 4.2.:

4.1 Non-ideal transfer gain of CCCTA

Considering the non-idealities of voltage, current and transconductance gains of CCCTA, the port relationship modifies as:

$$\begin{bmatrix} I_Y^{(1)} \\ V_X^{(1)} \\ I_Z^{(1)} \\ I_{O1}^{(1)} \\ I_{O2}^{(1)} \end{bmatrix} = \begin{bmatrix} 0 & 0 & 0 & 0 & 0 \\ \beta_1^{(1)} & 0 & 0 & 0 & 0 \\ 0 & \alpha_1^{(1)} & 0 & 0 & 0 \\ 0 & 0 & \gamma_1^{(1)} g_{m1}^{(1)} & 0 & 0 \\ 0 & 0 & 0 & \gamma_2^{(1)} g_{m2}^{(1)} & 0 \end{bmatrix} \begin{bmatrix} V_Y^{(1)} \\ I_X^{(1)} \\ V_Z^{(1)} \\ V_{O1}^{(1)} \\ V_{O2}^{(1)} \end{bmatrix} \quad (19)$$

While, the non-ideal port relationships of an EX-CCCTA are:

$$\begin{bmatrix} I_Y^{(2)} \\ V_{X1}^{(2)} \\ V_{X2}^{(2)} \\ I_{Z1}^{(2)} \\ I_{Z2}^{(2)} \\ I_{O1}^{(2)} \\ I_{O2}^{(2)} \end{bmatrix} = \begin{bmatrix} 0 & 0 & 0 & 0 & 0 & 0 & 0 \\ \beta_1^{(2)} & R_{X1}^{(2)} & 0 & 0 & 0 & 0 & 0 \\ \beta_2^{(2)} & 0 & R_{X2}^{(2)} & 0 & 0 & 0 & 0 \\ 0 & \alpha_1^{(2)} & 0 & 0 & 0 & 0 & 0 \\ 0 & 0 & \alpha_2^{(2)} & 0 & 0 & 0 & 0 \\ 0 & 0 & 0 & \gamma_1^{(2)} g_{m1}^{(2)} & 0 & 0 & 0 \\ 0 & 0 & 0 & 0 & \gamma_2^{(2)} g_{m2}^{(2)} & 0 & 0 \end{bmatrix} \begin{bmatrix} V_Y^{(2)} \\ I_{X1}^{(2)} \\ I_{X2}^{(2)} \\ V_{Z1}^{(2)} \\ V_{Z2}^{(2)} \\ V_{O1}^{(2)} \\ V_{O2}^{(2)} \end{bmatrix} \quad (20)$$

Where $\beta^{(i)}$ (i= 1, 2) is the voltage transfer gain between Y and $X^{(i)}$ terminals, $\alpha^{(i)}$ is the current transfer gain between $X^{(i)}$ and $Z^{(i)}$ terminals, $\gamma_1^{(i)}$ and $\gamma_2^{(i)}$ are the gains from $Z^{(i)}$ to $O_1^{(i)}$ and $O_1^{(i)}$ to $O_2^{(i)}$ terminals, respectively. The above gain factors are ideally found to be unity while practically they may slightly deviate from unity. After considering the non-ideality the transfer functions of Fig. 8 are obtained as:

$$\frac{I_{LP}}{I_{in}} = \frac{\gamma_1^{(1)}\gamma_2^{(1)}\alpha_1^{(1)}\alpha_1^{(2)}\alpha_2^{(2)}g_{m1}^{(1)}g_{m2}^{(1)}}{D(s)} \quad (21)$$

$$\frac{I_{BP}}{I_{in}} = \frac{sC_2\gamma_1^{(1)}\alpha_1^{(1)}\alpha_1^{(2)}\alpha_2^{(2)}g_{m1}^{(1)}}{D(s)} \quad (22)$$

$$\frac{I_{HP}}{I_{in}} = \frac{s^2C_1\alpha_1^{(1)}\alpha_1^{(2)}\alpha_2^{(2)}}{D(s)} \quad (23)$$

$$\frac{I_{BR}}{I_{in}} = \frac{\alpha_1^{(1)}\alpha_1^{(2)}\alpha_2^{(2)}\left(s^2C_1C_2 + \gamma_1^{(1)}\gamma_2^{(1)}g_{m1}^{(1)}g_{m2}^{(1)}\right)}{D(s)} \quad (24)$$

$$\frac{I_{AP}}{I_{in}} = \frac{\alpha_1^{(1)}\alpha_1^{(2)}\alpha_2^{(2)}\left(s^2C_1C_2 - sC_2\gamma_1^{(1)}g_{m1}^{(1)} + \gamma_1^{(1)}\gamma_2^{(1)}g_{m1}^{(1)}g_{m2}^{(1)}\right)}{D(s)} \quad (25)$$

Where,

$$D(s) = s^2C_1C_2\alpha_1^{(2)}\alpha_2^{(2)} + sC_2g_{m1}^{(1)}\gamma_1^{(1)}\alpha_1^{(1)}\alpha_2^{(2)}(\alpha_1^{(2)} + A_1\gamma_1^{(2)}) + \gamma_1^{(1)}\gamma_2^{(1)}\alpha_1^{(1)}\alpha_1^{(2)}g_{m1}^{(1)}g_{m2}^{(1)}(\alpha_2^{(2)} + A_2\gamma_2^{(2)}) \quad (26)$$

Therefore, the pole frequency (ω_o) and the quality factor (Q_o) are:

$$\omega_o = \sqrt{\frac{\gamma_1^{(1)}\gamma_2^{(1)}\alpha_1^{(1)}g_{m1}^{(1)}g_{m2}^{(1)}\left(\alpha_2^{(2)} + A_2\gamma_2^{(2)}\right)}{\alpha_2^{(2)}C_1C_2}} \quad (27a)$$

$$Q_o = \frac{\alpha_1^{(2)}}{\left(\alpha_1^{(2)} + A_1\gamma_1^{(2)}\right)}\sqrt{\frac{C_1g_{m2}^{(1)}\gamma_2^{(1)}\left(\alpha_2^{(2)} + A_2\gamma_2^{(2)}\right)}{C_2g_{m1}^{(1)}\gamma_1^{(1)}\alpha_1^{(1)}\alpha_2^{(2)}}} \quad (27b)$$

$$BW = \frac{g_{m1}^{(1)}\gamma_1^{(1)}\alpha_1^{(1)}\left(\alpha_1^{(2)} + A_1\gamma_1^{(2)}\right)}{\alpha_1^{(2)}C_1} \quad (27c)$$

From the Eq. (27), the effects due to non-idealities of CCCTA and EX-CCCTA can be easily observed. For the ideal cases, the current gains and transconductance gains are unity and Eq. (27) reverts to Eq. (14).

4.2 Effects of parasitics

Fig. 9 shows the non-ideal equivalent circuit of CCCTA and EX-CCCTA with parasitics. Series resistance at X terminal is of very low value while $\left(C_Y^{(1)} \parallel R_Y^{(1)}\right)$, $\left(C_Z^{(1)} \parallel R_Z^{(1)}\right)$, $\left(C_{O1}^{(1)} \parallel R_{O1}^{(1)}\right)$, and $\left(C_{O2}^{(1)} \parallel R_{O2}^{(1)}\right)$ are at Y, Z, O_1, and O_2 terminals, respectively. The values of $R_Y^{(1)}$, $R_Z^{(1)}$, $^{(\,)}$, and $R_{O2}^{(1)}$ are high whereas $^{(\,)}$, $C_Z^{(1)}$, $C_{O1}^{(1)}$, and $C_{O2}^{(1)}$ are low. The non-ideal circuit of the proposed shadow filter is shown in Fig. 10 where impedances are:

$$Z_1 = R_Z^{(1)} \left\| C_1^{'} \right., Z_2 = R_{O1}^{(1)} \left\| C_2^{'} \right.,$$
$$Z_3 = R_{O1}^{(1)} \left\| R_{Z1}^{(2)} \right\| C_{O1}^{(1)} \left\| C_{Z1}^{(2)} \right., \; Z_4 = R_{O2}^{(1)} \left\| R_{Z2}^{(2)} \right\| C_{O2}^{(1)} \left\| C_{Z2}^{(2)} \right. \quad (28)$$
$$Z_5 = R_{Z1}^{(2)} \left\| C_{Z1}^{(2)} \right., \; Z_6 = R_{Z2}^{(2)} \left\| C_{Z2}^{(2)} \right.$$

Where,

$C_1^{'} = C_1 + C_Z^{(1)}$ and $C_2^{'} = C_2 + C_{O1}^{(1)}$

The routine analysis of Fig. 10 results in the following TFs:

$$\frac{I_{LP}}{I_{in}} = \frac{g_{m1}^{(1)}g_{m2}^{(1)}}{D(s)} \quad (29)$$

$$\frac{I_{BP}}{I_{in}} = \frac{\left(sC_2^{'} + \frac{1}{R_{O1}^{(1)}}\right)g_{m1}^{(1)}}{D(s)} \quad (30)$$

$$\frac{I_{HP}}{I_{in}} = \frac{\left(sC_1^{'} + \frac{1}{R_Z^{(1)}}\right)\left(sC_2^{'} + \frac{1}{R_{O1}^{(1)}}\right)}{D(s)} \quad (31)$$

$$\frac{I_{BR}}{I_{in}} = \frac{\left(sC_1^{'} + \frac{1}{R_Z^{(1)}}\right)\left(sC_2^{'} + \frac{1}{R_{O1}^{(1)}}\right) + g_{m1}^{(1)} g_{m2}^{(1)}}{D(s)} \quad (32)$$

$$\frac{I_{AP}}{I_{in}} = \frac{\left(sC_1^{'} + \frac{1}{R_Z^{(1)}}\right)\left(sC_2^{'} + \frac{1}{R_{O1}^{(1)}}\right) + \left(sC_2^{'} + \frac{1}{R_{O1}^{(1)}}\right) g_{m1}^{(1)} + g_{m1}^{(1)} g_{m2}^{(1)}}{D(s)} \quad (33)$$

Where,

$$D(s) = \left(sC_1^{'} + \frac{1}{R_Z^{(1)}}\right)\left(sC_2^{'} + \frac{1}{R_{O1}^{(1)}}\right) + \left(sC_2^{'} + \frac{1}{R_{O1}^{(1)}}\right) g_{m1}^{(1)}\left(1 + A_1\right) + g_{m1}^{(1)} g_{m2}^{(1)}\left(1 + A_2\right) + E_1 + E_2 \quad (34)$$

Where,

$$E_1 = \frac{\left(sC_1^{'} + \frac{1}{R_Z^{(1)}}\right)\left(sC_2^{'} + \frac{1}{R_{O1}^{(1)}}\right) R_X A_1}{Z_3},$$

$$E_2 = \frac{\left(sC_1^{'} + \frac{1}{R_Z^{(1)}}\right)\left(sC_2^{'} + \frac{1}{R_{O1}^{(1)}}\right) R_X A_2}{Z_4}$$

From the Eq. (29) to (34), the effects of parasitics of CCCTA and EX-CCCTA on filters are observed. It may be noticed that the effects of parasitic capacitances can be neglected by choosing C_1 and C_2 much higher then C_Z and C_{01}. Moreover, as the values of R_Z and R_{01} are high, of the order of few MΩ, their effects are not significant for a few tens of MHz. It may also be found that the values of E_1 and E_2 are negligible in comparison to the other terms in Eq. (34) for a wide frequency range.

5 Comparison with existing CM SIMO Filters

As the proposed work is on CM SIMO UF, a fair comparison is carried out with available similar types of UFs. The comparison of the available CM single-input-multiple-output (SIMO) UF is given in Table 4. The filter topologies

(a)

(b)

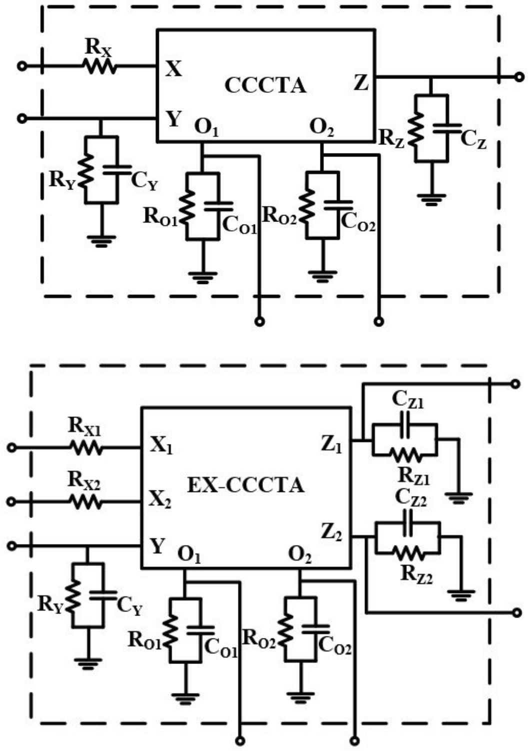

Figure 9: Non-ideal equivalent circuit of (a) CCCTA, (b) EX-CCCTA.

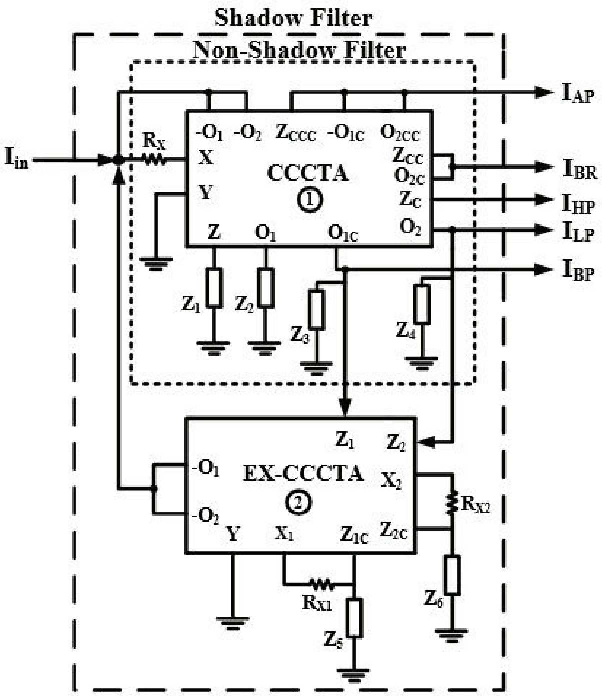

Figure 10: Non-ideal equivalent circuit of Fig. 8 with parasitic impedances.

[1-4, 8-28] are non-shadow (NS) type, while [29-35] are CM shadow (S) type. The filter topologies [8, 15, 24, 29-34, 35 (Fig. 9)] are single/multi-functional filters.

It is observed that topologies [1-4, 9-14, 16-23, 25-28, 35 (Fig. 10)] and proposed work are UFs. Whereas [26] is a direct realization using BJTs and excessive numbers of floating current sources. Its operating frequency is low, 100 kHz, and power consumption is 4.93mW. More than two analog building blocks (ABBs) are used in most UFs [1-4, 10, 12, 14, 17, 19-22, 35 (Fig. 10)], while the proposed shadow UF (SUF) uses two ABBs. Additionally, they suffer from one or more shortcomings as indicated in Table 4. It may be noted that topology [2]'s operating frequency is low, 39 kHz. Moreover, if the technique, as discussed in the paper [2], is applied for orthogonal tuning of ω_o and Q_o, then the AP filter will not work.

Furthermore, the UF topologies [11, 13, 16, 23, 25] use two ABBs. The UF topologies [11, 13, 16, 23] do not provide orthogonal tuning of ω_o and Q_o. Additionally, [11] has a low operating frequency and is not fully cascadable, while [16] does not provide simultaneous responses and independent tuning. The topology [23] uses two capacitors and three resistors, of which two are floating. Moreover, in [23], passive components matching constraints are required for UF realization. Further, unlike the proposed SUF, [23, 25] do not possess electronic tuning of ω_o and Q_o, and the full cascadability.

The UF topologies [9, 18, 27, 28] use one ABB compared to the two ABBs by the proposed SUF. However, the comparison Table 4 reveals that although these circuits use one ABB, the obtained current signals for HP and BP [9, 27] and that for HP [18, 28] conduct through series capacitors to ground, and hence they require significant additional circuitry for practical realization. As a consequence, for simultaneous realization, they need additional circuitry. As discussed in [18], the HP current can be made available from a high impedance terminal with one additional current conveyor and converting the corresponding grounded capacitor to a floating one. Moreover, [9, 18, 27, 28] are not cascadable without a buffer. Also, the power consumption is high in [27].

The power consumption of most of the available UFs is higher than the proposed work except [23, 35]. It is also noted that the operating frequency of 10 MHz and above is reported in [4, 10, 18, 21, 35], and the proposed work.

The above discussion establishes that the proposed SUF has advantage over all other UFs. Moreover, when we compare the proposed shadow filter with its own family (i.e., with available shadow filters), it is found that report of only one CM SUF [35 (Fig. 10)] is available. The proposed SUF is better than [35 (Fig. 10)] in terms of the number of ABBs used and also the fact that all capacitors are grounded compared to one floating capacitor in [35 (Fig. 10)]. Thus, in comparison to [35 (Fig. 10)], the proposed SUF consumes less space and is suitable for integrated circuit implementation.

6 Simulation results of the proposed SUF

The validation of the proposed circuit is performed with Cadence Virtuoso Spectre in TSMC 180 nm CMOS technology parameters. The layout of the SUF from Fig. 8 is shown in Fig. 11, which occupies an area of 110.35 µm x 73.6 µm. The supply voltages for CCCTA and EX-CCCTA are ± 1.5 V. The bias voltage V_{BB} is -1 V and bias currents are $I_{B1} = I_{B2} = 56$ µA for CCCTA whereas bias currents for EX-CCCTA are $I_{C1} = 100$ µA and $I_{C2} = I_{C3} = 56$ µA. The aspect ratio of transistors is given in Table 1 and Table 3 for CCCTA and EX-CCCTA respectively. The calculated frequency of 20.02 MHz, quality factor of 0.95 and bandwidth of 21.07 MHz are obtained for $C_1=C_2=1$ pf from Eq. (15). The filter gain responses such as LP, HP, BP, and BR for both the pre-layout and post-layout simulations are shown in Fig. 12 (a). Fig. 12 (b) shows the pre-layout and post-layout time response of the BP output for the input current of 50 µA, 20 MHz. Simultaneously, the gain and phase responses of the AP filter are shown in Fig. 13. The pole frequencies of the proposed filter for the pre-layout and post-layout are obtained as 20.2 MHz and 19.9 MHz, respectively. The deviation of post-layout pole frequency from pre-layout frequency is primarily due to parasitic capacitances.

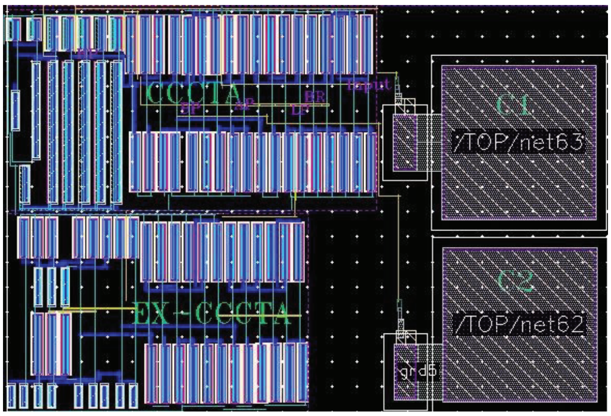

Figure 11: Layout of the proposed shadow universal filter (SUF) of Fig. 8.

The tunability of f_o by bias currents $I_{B1} = I_{B2}$ of CCCTA is shown in Fig. 14 for the SUF. The pre-layout simulated frequencies are obtained as f_o = 20.1 MHz, 37.6 MHz, and 53.5 MHz while the post-layout frequencies are obtained as f_o = 19.8 MHz, 37.01 MHz, and 53 MHz by varying the values of $I_{B1} = I_{B2}$ to 56 µA, 200 µA, and

Table 4: Comparative Study of available CM SIMO filters.

Ref.	No. and type of ABB used	Supply Voltage (V)	Passive elements (R,C)/ All grounded (Yes/N0)	Full cascadability	Filter functions/ Simulatneous responses (Yes/No)	Ease in independent adjustment of filter parameters fO and QO	Electronic tuning	Passive component matching constraint required	P.C. (mW)	Operating frequency (MHz)	S or NS filter
1.	4 CFTA	±3	2C / Yes	Yes	UF/ No	No	Yes	No	NA	0.153	NS
2.	2 CCCII, 1 MO-CCCA	±1.5	2C / Yes	Yes	UF/ Yes	Yes	Yes	No	NA	0.039	NS
3.	4 MO-OTA (Fig. 4)	±2	2C / Yes	No	UF/ Yes	Yes	Yes	Yes for UF realization	NA	0.238	NS
4.	3 DVCC	±2.5	4R, 2C/ Yes	No	UF/ Yes	No	No	Yes for UF realization	NA,	22.5	NS
8.	1 CFTA	±0.75	2C / Yes	No	LP, HP*, BP/ Yes	No	Yes	No	0.6	8	NS
9.	1 CCTA	±2	2R, 2C / Yes	No	UF*/ No	Yes	Yes	No	NA	1	NS
10.	3 DVCC, 6 MOS Resistor	±1.5	2C / Yes	Yes	UF/ No	Yes	No	Yes for UF realization	NA	16	NS
11.	2 OTA	NA	2C / Yes	No	UF/ Yes	No	Yes	No	NA	0.015	NS
12.	4 ZC-CFTA	±3	2C / Yes	Yes	UF/ Yes	Yes	Yes	No	12.2	0.159	NS
13.	2 ZC-CITA	NA	2C / Yes	Yes	UF/ Yes	No	Yes	No	NA	1.026	NS
14.	3 MOCCCII	±1.5	1R, 2C / Yes	No	UF/ Yes	No	Yes	No	NA	0.158	NS
15.	1 VDGA	±1	2R, 2C / No	No	LP, HP*, BP*/ Yes	No	Yes	No	1.49	1.59	NS
16.	2 EXCCTA	±1.25	4R, 2C / Yes	Yes	UF/ No	No	Yes	No	NA	7.62	NS
17.	3 DOCCCII (Fig. 2)	±2.5	2C / Yes	Yes	UF/ Yes	No	Yes	No	19.9	0.318	NS
	4 CCCII (Fig. 3)	±2.5	2C / Yes	Yes	UF/ Yes	No	Yes	No	NA	NA	NS
	3 CCCII (Fig. 4)	±2.5	2C / Yes	Yes	UF/ Yes	No	Yes	No	NA	NA	NS
18.	1 DXCCTA	±1.25	1R, 2C/ Yes	No	UF*/ Yes	No	Yes	No	NA	40	NS
19.	3 CCCII	±3	2C/ Yes	Yes	UF/ Yes	Yes	Yes	No	NA	0.127	NS
20.	3 ZC-CFTA	±1.5	2C/ Yes	Yes	UF/ Yes	Yes	Yes	No	NA	1.157	NS
21.	3 CCCII	±3	2C/ Yes	Yes	UF/ Yes	Yes	Yes	No	32	10	NS
22.	2 OTA, 1 CCIII	±1	1R, 2C/ Yes	Yes	UF/ Yes	Yes	Yes	No	NA	1	NS
23.	2 DVCC	±0.75	3R, 2C/ No	No	UF/ Yes	No	No	Yes for UF realization	0.81	3.18	NS
24.	1 VD-DXCC	±1.25	2R, 2C/ Yes	Yes	LP, HP, BP/ Yes	No	Yes	No	2.23	2.79	NS
25.	2 MO-OFC	±0.75	2R, 2C/ Yes	No	UF/ No	Yes	No	No	NA	1.5	NS
26.	BJT based	±2.7	2C/ Yes	NA	UF/ Yes	NA	Yes	No	4.93	0.1	NS
27.	1 VDTA	±1	1R, 2C/ Yes	No	UF*/ No	Yes	Yes	No	19	7	NS
28.	1 EXCCTA	±0.9	1R, 2C/ Yes	No	UF*/ No	No	Yes	No	NA	2.204	NS
29.	2 CDTA, 1TA	±1.8	1R, 2C/ Yes	No	LP*, BP/ Yes	Yes	Yes	No	21.2	9.95	S
	2 VDTA	±1.8	2C/ Yes	No	LP, BP*/ Yes	Yes	Yes	No	17.4	5.625	S
30.	2 CDTA	±1.8	2R, 2C, No	No	BP*/ Yes	No	No	No	7.79	4	S
31.	3 CDTA	±0.9	1R, 2C, Yes	No	LP, HP*, BP*/ Yes	No	Yes	No	5.9	15.1	S
32.	4 OFCC	±1.5	5R, 2C, Yes	Yes	BP/ Yes	Yes	No	No	NA	1.59	S
33.	2 CDTA, 1CA	±0.9	2C/ Yes	Yes	BP/ Yes	Yes	Yes	No	NA	1	S
34.	4 ECCII	±0.9	2R, 2C/ No	No	BP/ Yes	No	No	No	NA	19.05	S
35.	2 CC-CDCTA (Fig. 9)	±1.25	2C/ Yes	No	LP, HP*, BP/ Yes	Yes	Yes	No	1.5	79.8	S
	3 CC-CDCTA, 1 CCII (Fig. 10)	±1.25	2C/ No	Yes	UF/ Yes	Yes	Yes	No	2.23	79.8	S
Prop. Work	1 CCCTA, 1 EX-CCCTA	±1.25	2C/ Yes	Yes	UF/ Yes	Yes	Yes	No	4.1	20.02	S

*Indicates the obtained current signal for the respective response conducts through a grounded capacitor and/or resistor, hence additional circuitry is required for practical application; NA: Not available; PC: Power Consumption; Full Cascadability: Cascadable both at the input and output, S: Shadow; NS: Non-shadow; CA: Current amplifier

(a)

(b)

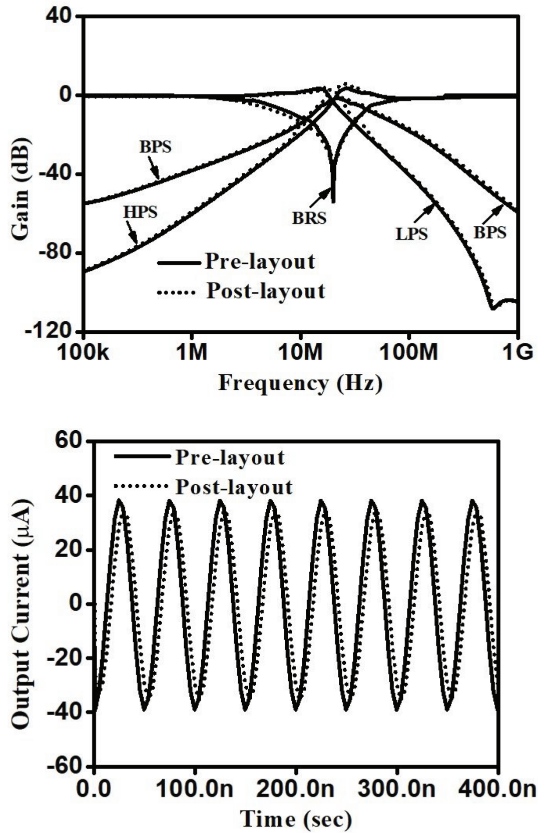

Figure 12: Simulated results (a) gain responses of the SUF for HP, LP, BP, and BR (b) time response of BP output..

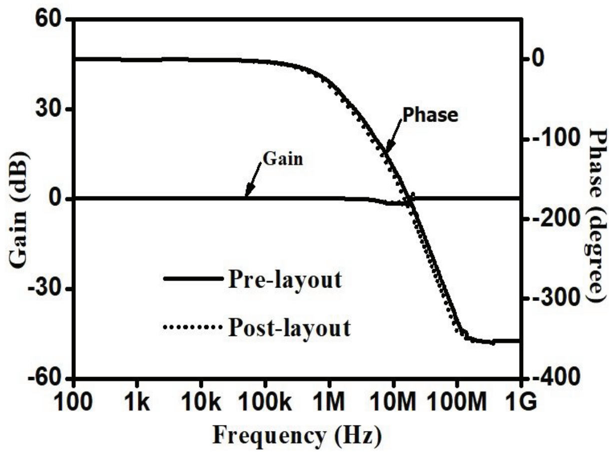

Figure 13: Simulated results of gain and phase response for the all-pass (AP) filter

400 µA, respectively. Whereas the calculated values of frequencies are 20.02 MHz, 37.8 MHz, and 53.49 MHz with a deviation of 1.09%, 2%, and 0.9%, respectively in comparison with post-layout frequencies, for the fixed quality factor. Similarly, the pre-layout simulated bandwidths are 19.7 MHz, 36.86 MHz, and 52.4 MHz vis-à-vis the calculated bandwidths of 20.02 MHz, 37.8 MHz, and 53.49 MHz, respectively. While the post-layout bandwidths are 19.22 MHz, 35.93 MHz, and 51.45 MHz with a deviation of 3.9%, 4.9%, and 3.8%, respectively.

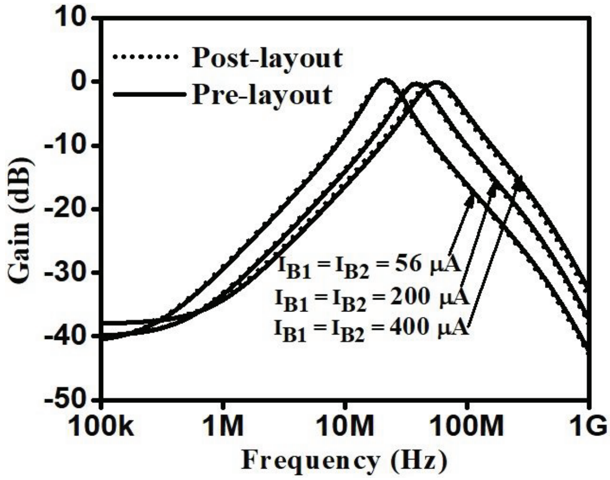

Figure 14: Simulated results of tuning of f_O by varying bias currents (I_{B1} & I_{B2}) of CCCTA for fixed Q_O.

Furthermore, as given in Eq. (15), f_o can also be tuned along with BW without changing the quality factor by varying C_1=C_2=C. The pre-layout simulated responses are shown in Fig. 15, resulting in f_o = 20.1, 9.9, and 2.48 MHz for the capacitor value of C_1=C_2= 1 pF, 2 pF, and 8 pF, respectively while the post-layout frequencies are 19.62, 9.75, and 2.45 MHz, respectively. In contrast, the calculated results are obtained as 20.02, 10.01, and 2.5 MHz with a deviation of 1.9%, 2.5%, and 2%, respectively, for a fixed calculated quality factor of 1. Similarly, the pre-layout simulated bandwidths are 19.7 MHz, 9.7 MHz, and 2.45 MHz and the post-layout bandwidths are 19.23 MHz, 9.6 MHz, and 2.43 MHz for the calculated bandwidths of 20.02 MHz, 10.01 MHz 2.5 MHz, respectively, with a deviation of 3.9%, 4%, and 2.8%.

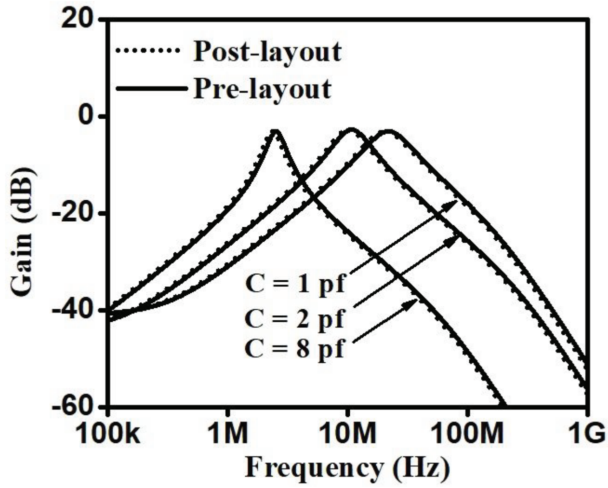

Figure 15: Simulated results of tuning of f_O by varying capacitance value C for fixed Q_O.

The tuning of the quality factor (Q_o) with A_1 (i.e., $g_{m1}^{(2)}$ or I_{C2} of EX-CCCTA) without changing f_o, as per Eq. (15), is validated in Fig. 16 for band pass response. The responses are obtained by varying bias current I_{C2} = 56, 200, and 400 μA of EX-CCCTA. The corresponding pre-layout simulated quality factors are obtained as Q_o = 1.58, 1.27, 0.96, the post-layout quality factors are obtained as Q_o = 1.6, 1.3, 0.97 vis-a-vis calculated values as 1.55, 1.25, 0.95 with a deviation of 3.2%, 4%, and 2.1% respectively.

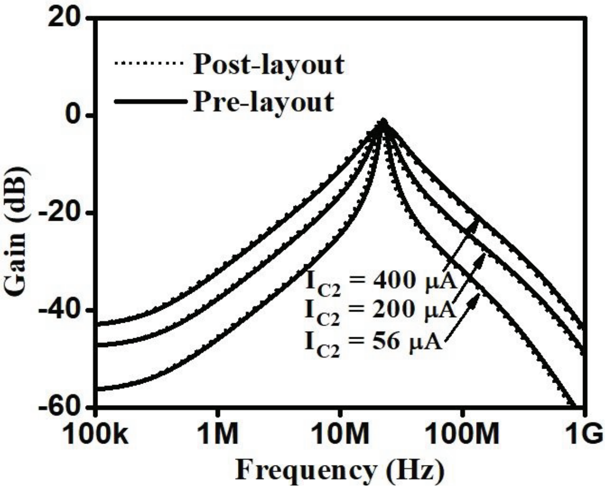

Figure 16: Simulated results of tuning of Q_O by varying A_1 with I_{C2} of EX-CCCTA for fixed f_O.

The tuning of the f_o and Q_o without disturbing BW by varying A_2 (i.e., $g_{m2}^{(2)}$ or I_{C3} of EX-CCCTA) is verified in Fig. 17. For the bias currents I_{C3} = 56, 200, 400 μA, the pre-layout simulated frequencies resulted in 19.8, 21.3, and 23.52 MHz while, the post-layout frequencies are 19.5, 20.9, and 23.2 MHz vis-à-vis the calculated frequencies of 20.02, 21.55, 23.55 MHz with a respective deviation of 2.5%, 3%, and 1.9%. Similarly, the pre-layout simulated quality factors are obtained as 0.94, 1.014, and 1.1 while the post-layout quality factors are 0.93, 1.01, and 1.09 for the calculated quality factors of 0.95, 1.022, and 1.117 with a deviation of 2.4%, 1.1%, 1.8%. The pre-layout and post-layout simulated BW was 21 MHz and 20.9, respectively vis-à-vis calculated BW of 21.07 MHz.

The measure of %THD (Total Harmonic Distortion) for the HP and LP responses as a function of the input signal is given in Fig. 18. It is observed that %THD is low up to 1 mA. The intermodulation distortion (IMD) for the BP filter is simulated using the sinusoidal input signal of 100 μA, 10 MHz with an addition of parasitic sinusoidal signal of 10 μA for the respective frequencies as given in Table 5. The output noise of the BP filter has also been studied, as shown in Fig. 19. The pre-layout and post-layout noise of the shadow filter is 21 aA²/Hz and 21.4 aA²/Hz at 1 Hz, and after that, it decays exponentially. Eq. (35) gives the calculation of dynamic range, where the graphical integration of the squared spectrum is obtained from Fig. 19 and the maximum linear swing of the output ($I_{OL, max}$), approximately 180 μA and 176 μA, are obtained from Fig. 20 for the pre-layout and the post-layout respectively. The resulted pre-layout and post-layout dynamic ranges are 75.6 dB and 71.5 dB, respectively.

$$Dynamic\ Range = 20 * log_{10} \frac{I_{OL,\ max}}{\sqrt{Int.of\ squared\ spectrum}} \quad (35)$$

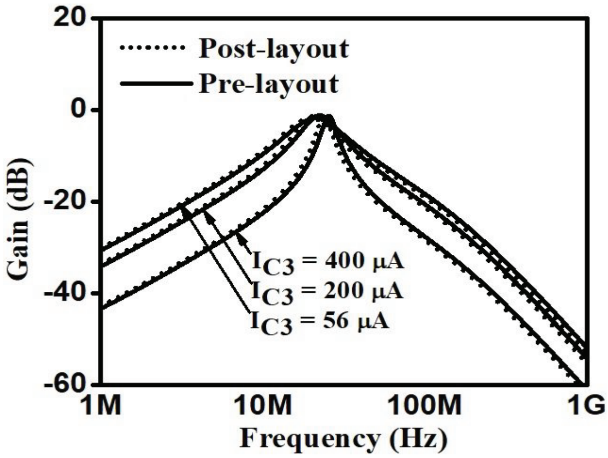

Figure 17: Simulated results of tuning of f_O and Q_O by varying A_2 with I_{C3} of EX-CCCTA.

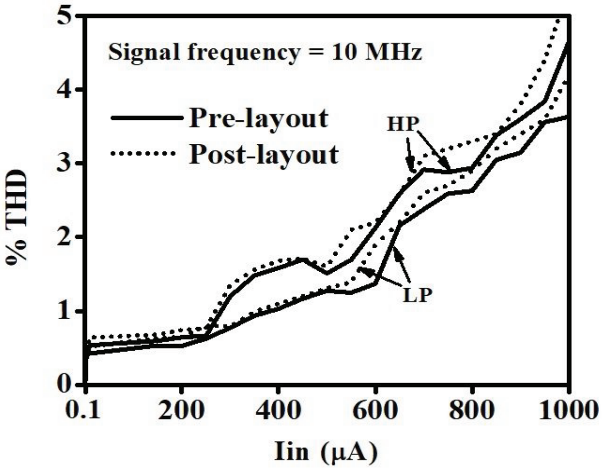

Figure 18: %THD Variation of HP and LP filter.

Table 5: IMD results for the band pass filter.

Frequency for the parasitic signal (MHz)	1	5	8	10	15	18	20	25
% THD	1.61	0.74	1.26	1.68	1.17	1.73	2.91	2.45

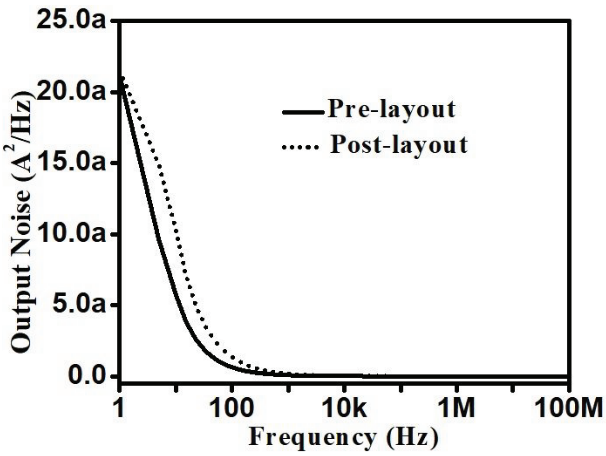

Figure 19: Output noise for the BP.

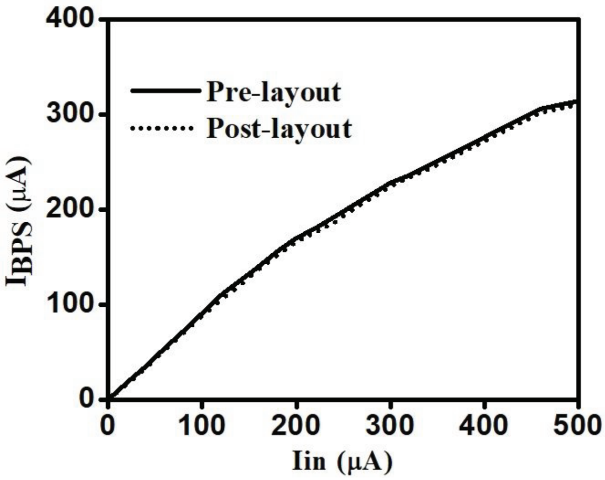

Figure 20: Transfer linearity test for BP output signal.

7 Conclusions

This paper started with presenting two new active building blocks, CCCTA and EX-CCCTA, which are the modified versions of CCTA and EX-CCCII, respectively. The proposed SUF uses only two grounded capacitors and no resistor. It is free from any matching constraints. All the standard responses such as LP, BP, HP, BR, and AP are obtained simultaneously without altering the SUF circuit. It provides the possibility to orthogonally adjust the pole frequency and the quality factor in comparison to NSUF. Moreover, the electronic tuning of filter's various parameters can be performed conveniently. Input and output impedances are low and high, respectively, which makes the filter fully cascadable. Power consumption is found to be low compared to most of the filters in available literature. The theoretical results were verified with post layout simulation in Cadence Virtuoso using TSMC 180 nm technology.

8 Conflict of interest

The authors declare that there is no conflict of interest for this paper. Also, there are no funding supports for this manuscript.

9 References

1. W. Tangsrirat, "Single-input three-output electronically tunable universal current-mode filter using current follower transconductance amplifiers," AEU-Int. J. Electron. Commun., vol. 65, n0. 10, pp. 783-787, Oct. 2011, https://doi.org/10.1016/j.aeue.2011.01.002.
2. C. Wnag, J. Xu, A. U. Keskin, S. Du, and Q. Zhang, "A new current-mode current-controlled SIMO type universal filter," AEU-Int. J. Electron. Commun., vol. 65, n0. 3, pp. 231-234, Mar. 2011, https:doi.org/10.1016/j.aeue.2010.02.010.
3. D. V. Kamat, P. V. A. Mohan, and K. G. Prabhu, "Novel first-order and second-order current-mode filters using multiple-output operational transconductance amplifiers," Circuits Systems and Signal Processing, vol. 29, pp. 553-576, Mar. 2010, https://doi.org/10.1007/s00034-010-9163-y.
4. M. A. Ibrahim, S. Minaei, and H. A. Kuntman, "22.5 MHz current-mode KHN-biquad using differential voltage current conveyor and grounded passive elements," AEU-Int. J. Electron. Commun., vol. 59, no. 5, pp. 311-318, Jul. 2005, https://doi.org/10.1016/j.aeue.20o4.11.027.
5. Y. Lakys, and A. Fabre, "Shadow filters-new family of second order filters," Electronics Letters, vol. 46, no. 4, pp. 276-277, Feb. 2010, https://doi.org/10.1049/el.2010.3249.
6. Y. Lakys, and A. Fabre, "Shadow filter generalization to nth class," Electronics Letters, vol. 46, no. 14, pp. 985-986, Jul. 2010, https://doi.org/10.1049/el.2010.0452.
7. V. Biolkova, D. A. Biolek, "Shadow filters for orthogonal modification of characteristic frequency and bandwidth," Electronics Letters, vol. 46, no. 12, pp. 830-831, Jun. 2010.
8. S. V. Singh, R. S. Tomar, and D. S. Chauhan, "Single CFTA based current-mode universal biquad filter," The Journal of Engineering Research, vol. 13, no. 2, pp. 172-186, May 2016, https://doi.org/10.24200/tjer.vol13iss2pp172-186
9. N. Herencsar, J. Koton, and K. Vrba, "Single CCTA-based universal biquadratic filters employing minimum components," International Journal of Computer and Electrical Engineering, vol. 1, no.3, pp. 307-310, Aug. 2009.

10. S. Minaei, and M. A. Ibrahim, "A mixed-mode KHN-biquad using DVCC and grounded passive elementssuitable for direct cascading," International Journal of Circuit Theory and Applications, vol. 37, pp. 793-810, https://doi.org/10.1002/cta.493.
11. A. Qadir, and T. Altaf, "Current mode canonic OTA-C universal filter with single input and multiple outputs," In: Proceedings of International Conference on Electronic Computer Technology (ICECT' 10), pp. 32-34, Jun. 2010, https://doi.org/10.1109/ICECTECH.2010.5479995.
12. J. Satansup, and W. Tangsrirat, "Single-input five-output electronically tunable current-mode biquad consisting of only ZC-CFTAs and grounded capacitors," Radioengineering, vol. 20, no. 3, pp. 650-656, Sep. 2011.
13. D. Biolek, V. Biolkova, Z. Kolka, and J. Bajer, "Single-input multi-output resistorless current-mode Biquad," In: Proceedings of IEEE European Conference on Circuit Theory and Design, pp. 225-228, Oct. 2009, https://doi.org/10.1109/ECCTD.2009.5274928.
14. R. Senani, V. K. Singh, A.K. Singh, D.R. Bhaskar, "Novel electronically controllable current-mode universal biquad filter," IEICE Electron Express 1, vol. 1, no. 14, pp. 410-415, Oct. 2004, https://doi.org/10.1587/elex.1.410.
15. W. Tangrirat, T. Pukkalanun, and O. Channumsin, "Single VDGA-based dual-mode multifunction biquadratic filter and quadrature sinusoidal oscillator," Informacije MIDEM, vol. 50, no. 2, pp. 125-136, 2020, https://doi.org/10.33180/InfMIDEM2020.205.
16. M. I. A. Albrni, F. Mohammed, N. Herencsar, J. Sampe, and S. H. M. Ali, "Novel electroniacally tunable biquadratic mixed mode universal filter capable of operating in MISO and SIMO configurations," Informacije MIDEM, vol. 50, no. 3, pp. 189-203, 2020, https://doi.org/10.33180/InfMIDEM2020.304
17. E. Yuce, "Current-mode electronically tunable biquadratic filters consisting of only CCCIs and grounded capacitors," Microelectronics Journal, vol. 40, no. 12, pp. 1719-1725, Dec. 2009, https://doi.org/10.1016j.mejo.2009.09.002.
18. A. Kumar, B. Chaturvedi, "Novel CMOS dual-X current conveyor transconductance amplifier realization with current-mode multifunction filter and quadrature oscillator," Circuits Systems and Signal Processing, vol. 37, pp. 2250-2277, Oct. 2017, https://doi.org/10.1007/s00034-017-0680-9.
19. M. Kumngern, "A new current-mode universal filter with single-input five-output using translinear current conveyors," Australian Journal of Eectrical and Electronics Engineering, vol. 9, no. 2, pp. 177-184, Sep. 2015, https://doi.org/10.1080/1448837X.2012.11464322
20. B. Singh, A. K. Singh, and R. Senani, "New universal current-mode biquad using only three ZC-CFTAs," Radioengineering, vol. 21, no. 1, pp. 273-280, Apr. 2012.
21. M. Kumngern, P. Phasukkit, S. Junnapiya, F. Khateb, and S. Tugjitkusolmun, "ECCCII-based current-mode universal filter with orthogonal control of w_o and Q," Radioengineering, vol. 23, no. 2, pp. 687-696, Jun. 2014.
22. T. S. Arora, M. Gupta, S. Gupta, "Current mode universal filter employing operational transconductance amplifier and third generation current conveyor," In: IEEE International Conference on Power Electronics, Intelligent Control and Energy Systems (ICPEICES), IEEE, pp. 1-4, Feb. 2017, https://doi.org/10.1109/ICPEICES.2016.7853305.
23. A. Abaci, and E. Yuce, "A new DVCC+ based second-order current mode universal filter consisting of only grounded capacitors," Journal of Circuits Systems and Computers, vol. 26, no.9, pp. 1750130, Feb. 2017, https://doi.org/10.1142/S0218126617501304.
24. M. A. Albrni, M. Faseehuddin, J. Sampe, and S. H. M. Ali, "Novel dual mode multifunction filter employing highly versatile VD-DXCC," Informacije MIDEM, vol. 49, no. 3, pp. 169-176, 2019, https://doi.org/10.33180/InfMIDEM2019.305.
25. T. Praveen, "OFC based high output impedance current mode SIMO universal biquadratic filter," In: International Conference on Multimedia Signal Processing and Communication Technologies (IMPACT), IEEE, pp. 134-136, Feb. 2012, https://doi.org/10.1109?MSPCT.2011.6150456
26. R. Arslanalp, E. Yuce, and T. A. Tola, "Two lossy integrator loop based current-mode electronically tunable universal filter employing only grounded capacitors," Microelectronics Journal, vol. 59, pp. 1-9, Jan. 2017, https://doi.org/10.1016/j.mejo.2016.11.005.
27. D. Prasad, D. R. Bhaskar, and M. Srivastava, "Universal current-mode biquad filter using a VDTA," Circuits and Systems, vol. 4, pp. 29-33, Jan. 2013, https://dx.doi.org/10.4236/cs.2013.41006.
28. M. Faseehuddin, J. Sampe, S. Shireen, S. H. M. Ali, "Lossy and lossless inductance simulators and universal filters employing a new versatile active block," Informacije MIDEM, vol. 48, no. 2, pp. 97-113, 2018.
29. N. Pandey, A. Sayal, R. Choudhary, and R. Pandey, "Design of CDTA and VDTA based frequency agile filters," Advances in Electronics, vol. 2014, pp. 1-14, Dec. 2014, https://doi.org/10.1155/2014/176243.

30. N. Pandey, R. Pandey, R. Choudhary, A. Sayal, and M. Tripathi, "Realization of CDTA based frequency agile filters," IEEE International Conference on Signal Processing, Computing and Control, pp. 1-8, Nov. 2013, https://doi.org/10.1109/ISPCC.2013.6663403.
31. M. Atasoyu, H. Kuntman, B. Metin, N. Herencsar, and O. Cicekoglu, "Design of current-mode class 1 frequency agile filter employing CDTAs," European Conference on Circuit Theory and Design, pp. 1-4, Oct. 2015, https://doi.org/10.1109/ECCTD.2015.7300066.
32. D. Nand, and N. Pandey, "New configuration for OFCC-based CM SIMO filter and its application as shadow filter and its application as shadow filter," Arabian Journal for Science and Engineering, vol. 43, no. 6, pp. 3011-3022, June. 2018, https://doi.org/10.1007/s13369-017-3058-1.
33. A. Yesil, and F. Kacar, "Band-pass filter with high quality factor based on current amplifier," AEU-Int. J. Electron. Commun., vol. 75, pp. 63-69, May 2017, https://doi.org/10.1016/j.aeue.2017.03.007.
34. M. Atasoyu, B. Metin, H. Kuntman, and N. Herencsar, "New current-mode class 1 frequency-agile filter for multi-protocol GPS application," Elektronica ir Elektrotechnika, vol. 21, no. 5, pp. 35-39, May 2015, https://doi.org/10.5755/j01.eee.21.5.13323.
35. D. Singh, and S. K. Paul, "Realization of current mode universal shadow filter," AEU-Int. J. Electron. Commun., vol. 117, pp. 1-16, Apr. 2020, https://doi.org/10.1016/j.aeue.2020.153088
36. F. Khateb, W. Jaikla, T. Kulej, M. Kumngern, and D. Kubanek, "Shadow filters based on DDCC," IET Circuits Devices Syst., vol. 11, pp. 631-637, Oct. 2017, https://doi.org/10.1049/iet-cds.2016.0522.
37. S. C. Roy, "Shadow filters: a new family of electronically tunable filters," IETE J. Edu., vol. 51, pp. 75-78, Sep. 2014, https://doi.org/10.1080/09747338.2010.10876070
38. M. T. Abuelma'atti, N. R. Almutairi, "New current-feedback operational amplifier based shadow filters," Analog Integr. Circ. Sig. Process., vol. 86, pp. 471-480, Jan. 2016, https://doi.org/10.1007/s10470-016-0691-7.
39. M. T. Abuelma'atti, N. Almutairi, "New voltage-mode bandpass shadow filters," In: 13th International multi-conference on systems, signals & devices, pp. 412-415, May 2016, https://doi.org/10.1109/SSD.2016.7473695.
40. M. T. Abuelma'atti, N. Almutairi, "New CFOA-based shadow bandpass filters," In: 15th International conference on electronics information, and communications, Sep. 2016, https://doi.org/10.1109/ELINFOCOM.2016.7562969.
41. R. Anurag, R. Pandey, N. Pandey, M. Singh, and M. Jain, "OTRA based shadow filters," Annual IEEE India Conference, Mar. 2016, https://doi.org/10.1109/INDICON.2015.7443524.
42. P. Huaihongthong, A. Chaichana, P. Suwanjan, S. Siripongdee, W. Sunthonkanokpong, P. Supavarasuwat, W. Jaikla, and F. Khateb, "Single-input multiple-output voltage-mode shadow filter based on VDDDAs," AEU-Int. J. Electron. Commun., vol. 103, pp. 13-23, May 2019, https://doi.org/10.1016/j.aeue.2019.02.013.
43. A. Yesil, F. Kacar, and S. Minaei, "Electronically controllable bandpass filters with high quality factor and reduced capacitor value: an additional approach," AEU-Int. J. Electron. Commun., vol. 70, pp. 936-943, Jul. 2016, https://doi.org/10.1016/j.aeue.2016.04.009.
44. T. Thosdeekoraphat, S. Summart, C. Saetiaw, S. Santalunai, and C. Thogsopa, "CCCTAs based current-mode quadrature oscillator with high output impedances," International Journal of Electronics and Electrical Engineering, vol. 1, no. 1, pp. 52-56, Jan. 2013.
45. D. Agrawal, and S. Maheshwari, "Current mode filters with reduced complexity using a single EX-CCCII," AEU-Int. J. Electron. Commun., vol. 80, pp. 86-93, Oct. 2017, https://doi.org/10.1016/j.aeue.2017.06.025.

Arrived: 14. 11. 2021
Accepted: 04. 03. 2022